Electronic Supplementary Material (ESI) for Analyst

Supporting Information for Quantification of noise sources for amperometric measurement of quantal exocytosis using microelectrodes

Jia Yao[1,2] and Kevin D. Gillis[1,2,3]

[1]Department of Biological Engineering, [2]Dalton Cardiovascular Research Center, [3]Department of Medical Pharmacology and Physiology, University of Missouri, Columbia, MO

SUPPORTING INFORMATION ABSTRACT

Details concerning the processes used for electrode fabrication and testing are presented in the Supporting Experimental Section. The Supporting Results Section presents experiments that demonstrate electrode responses with a test analyte and a plot of electrode capacitance versus area. Results are presented demonstrating that the noise standard deviation increases with the square-root of electrode area for small electrodes, but increases linearly with area for larger electrodes. The Supporting Discussion Section provides elaboration on possible noise sources for amperometric measurements using microelectrodes and summarizes strategies for reducing noise during amperometric recording of exocytosis.

SUPPORTING INFORMATION EXPERIMENTAL SECTION

Fabrication of electrochemical microelectrodes

ITO coated glass slides (film thickness 15-30 nm with a sheet resistance of 70-100 Ω) were purchased from Sigma (St. Louis, MO, USA) or deposited using a magnetron sputtering system (ATC2000, AJA International Inc., North Scituate, MA, USA) as previously described[1]. Au (~20 nm thick) was sputter deposited on a ~2 nm adhesion layer of Ti, whereas DLC:N (~100 nm thick) was sputter deposited on top of ITO in order to reduce the sheet resistance as previously described[2].

Electrode materials were patterned using etching processes with S1813 photoresist (Rohm and Haas electronic materials, Philadelphia, PA, USA) as the masking material. First, the conductor-coated slides were cleaned by sonication in acetone for 10 minutes followed by exposure to air plasma (PDC-32G, Harrick Scientific Corp., Pleasantville, NY, USA) for 1 min at medium RF power level. S1813 photoresist was then spin coated (Laurell Technologies Corp., North Wales, PA, USA) onto the coated slide at 2500 rpm for 60 seconds to give a thickness of ~2 μm. The coated glass slide was then baked on a hot plate at 115 ℃ for 2 minutes. Then it was exposed to UV light through a high-resolution (20,000 dpi) transparency mask (CAD/Art services, Inc. Bandon, OR) for about 43 seconds (NuArc 26-1KS Exposure unit, 1000 W metal halide lamp, 5.4 mW/cm^2) and then developed in M351 solution (Rohm and Haas electronic materials) for ~1 min.

ITO films were wet etched using a solution composed of 6 M HCl and 0.2 M $FeCl_3$ for 30 minutes. Au films were wet etched using Au etching reagent purchased from Sigma-Aldrich for ~ 5 s. DLC:N films were etched using 10 minute exposure to air plasma using the high power setting of the PDC-32G.

Following removal of the S1813 with acetone, the conductive films were patterned into 36 stripes with widths of either ~40 μm or ~100 μm. Each stripe leads to a 2 mm diameter pad at the edge of the chip to facilitate connection to a potentiostat (Fig. 1B). The stripes were insulated with photoresist (S1813 or SU8 2025) except for small openings that defined the area of each of the 36 working electrodes.

S1813 photoresist insulation was processed similar to the method described above, with hard baking at 150 ℃ for 10 min in order to make a harder film. When SU8 2025 was used as the insulating material, it was first spin coated onto the device at 4000 rpm for 1 min to give a thickness of ~16 μm. Then it was baked on a hot plate at 65 ℃ for 3 min and then 95 ℃ for 5 min. The SU-8 was exposed through the photomask for ~33 s and then developed in SU8 developer for ~10 min. Afterwards it was baked again at 65 ℃ for 1 min and 95 ℃ for 5 min. Finally it was hard baked at 150 ℃ for 30 min to harden the film and seal cracks.

A polydimethylsiloxane (PDMS, Sylgard 184, Dow Corning, Midland, MI. USA) gasket was sealed onto the device to hold the bath solution. A custom-built chamber was used to hold the microchip device and to facilitate connection of the potentiostat to the pads at the edge of the chip. A Ag/AgCl wire was immersed in the drop of bath solution to serve as the reference electrode.

Cleaning the working electrode was important to ensure an active surface. Before use, the device was rinsed with deionized water, air dried and then treated with air plasma at the medium power setting for 30 s to etch any photoresist residue on the electrode surface. For the chip insulated with SU8, a 30-min incubation in 30% H_2O_2 /1M KOH was applied followed by rinse in deionized water rinse and air drying.

Current Power Spectral Density (PSD) measurements

The current signal was low-pass filtered with a 4-pole Bessel filter set to a corner frequency of either 3 kHz or 5 kHz and sampled at 20 ksamples/s. The current power spectral density for 20 s of sampled data was calculated using Igor software (Wavemetrics, Inc., Lake Oswego, OR). Data were processed with a segment length of 8192 samples and a square window to preserve low frequency information. In order to reduce line interference, devices were shielded and a Humbug instrument (Quest Scientific, North Vancouver, BC, Canada) was used in some experiments to remove 60 Hz and harmonics from the signal. To further ensure the removal of line interference, a custom-developed Igor macro was applied to subtract 60 Hz and harmonics obtained from a training portion of the signal. Five current recordings were made from each electrode and the resulting PSDs were averaged.

Admittance measurements

A software lock-in amplifier[3] integrated within PULSE software (HEKA) was used to measure admittances. Attenuation and phase shifts introduced within the amplifier were corrected using a manual calibration procedure. A 40 pF capacitor was inserted into the headstage to serve as a 90° phase reference, and the phase offset and each test frequency was obtained. Admittance measurements were made with a stimulus sinusoid with an amplitude of 25 mV and with frequencies ranging between 5 Hz and 5 kHz at log intervals. The 10-kHz Bessel filter was used to low-pass filter the current, and the sampling rate was fixed at 20 ksamples/s. The constant phase element model parameters were obtained by fitting the admittance data using a Levenberg-Marquardt algorithm in Igor to minimize the sum of the squared error of the real and imaginary admittances. Electrode capacitance was measured using the software lock-in amplifier with the "Sine+DC" method[3-5]with a 25 mV amplitude sinusoid at a frequency of 1 kHz.

SUPPORTING INFORMATION RESULTS SECTION

Confirmation of electrode sensitity with cyclic voltammetry

Cyclic voltammetry with the test analyte ferricyanide $K_3Fe(CN)_6$ (1 mM in 0.1 M KCl, pH 3.0) was used to confirm the electrochemical activity of each electrode before use. Sample cyclic voltammograms are presented in Fig. S-1. The CF electrode was ~8 μm in diameter whereas the planar electrodes were ~20 μm in diameter. As the potential becomes more negative than ~0.15 V (versus Ag/AgCl), a sharp transition to an anodic current was evident as ferricyanide was reduced on the surface of the electrode. This indicates the series resistance of the electrode was acceptable and there were no significant offset potentials. For slow scans at anodic potentials the current reached a plateau (i_{lim}) that was determined by the rate that ferricyanide diffuses to the electrode surface. For a disk electrode on an infinite insulating plane, the diffusion-limited current for monovalent electron transfer is given by[6]:

$$i_{lim} = 4FDCr$$

where *F* is Faraday's constant, *D* is the diffusion coefficient for ferricyanide (~7.2×10^{-6} cm^2 s^{-1}), *C* is the concentration of ferricyanide (1 mM) and *r* is the radius of the electrode. Thus i_{lim} can be used to confirm that the effective electrode size is as expected. The predicted values of i_{lim} are ~1.1 nA and 2.8 nA for electrodes with diameters of 8 μm and 20 μm, respectively, therefore the measured values confirm the effective sizes of the electrodes were roughly as expected and the insulating film was intact. Some electrode-to-electrode variability in i_{lim} and double-layer capacitance was observed presumably due to limitations of precision of our photolithographic equipment.

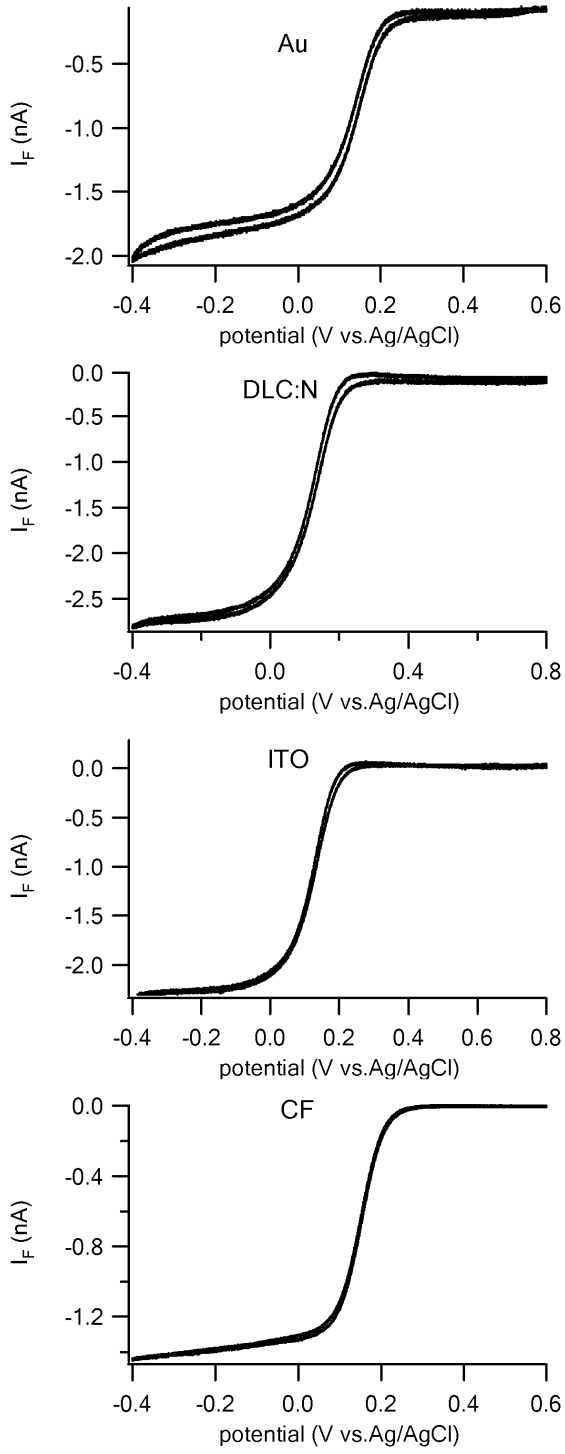

Fig. S-1. Sample Cyclic Voltammograms with the test analyte ferricyanide demonstrate electrodes fabricated from the various materials are electrochemically active, are well-insulated and are approximately the expected area. The Au, DLC:N and ITO electrodes had a diameter of ~20 μm, whereas the CF electrode had a diameter of ~8 μm. The scan rate was 10 mV/s.

The capacitance per unit area is similar among the sputter-deposited materials

As described in the Experimental Section, Au, DLC:N and ITO were deposited on glass substrates using magnetron sputtering to yield atomically smooth electrodes verified using atomic force microscopy[7]. Electrodes of various areas were fabricated as described and the capacitance of each electrode was measured at a frequency of 1 kHz. The area of each electrode was also estimated using a microscope. Figure S-2 is a plot of the background-subtracted capacitance versus area for the three materials whereas the line depicts the best-fit slope of 0.077 pF/μm^2. Note that the capacitance per unit area is roughly similar among the materials, which is consistent with a similar smoothness of the electrode surfaces. Individual linear fits to data obtained from each material yielded slopes of 0.094, 0.077 and 0.072 pF/μm^2 for DLC:N, ITO and Au, respectively. It should be noted that several-fold larger capacitances will be obtained using lower test frequencies or by using time-domain methods to measure capacitance because the impedance of electrochemical electrodes is best described by a CPE model rather than an ideal capacitance.

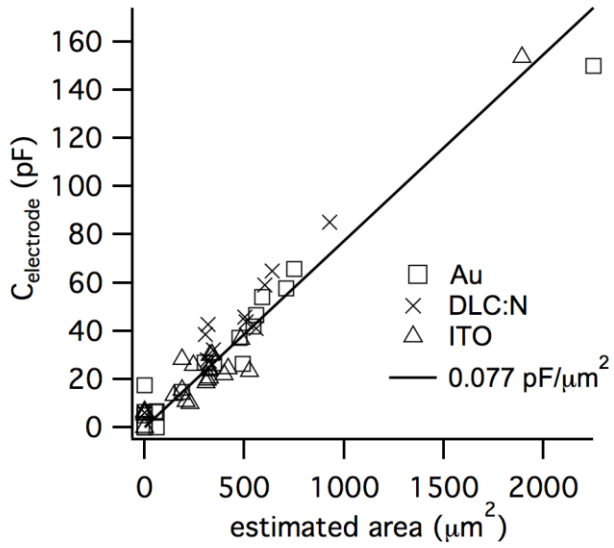

Fig. S-2. Plot of electrode capacitance versus area for planar electrodes fabricated from Au (squares), DLC:N (Xs) and ITO (triangles).

The noise standard deviation (σ_I) increases approximately linearly with electrode area for working electrode areas greater than ~3000 μm^2.

As demonstrated in Fig. 6A, σ_I increase approximately with the square-root of electrode area for electrodes smaller than 2500 μm^2, which is the expected relationship if thermal noise dominates (Eq. 9). However, σ_I has previously been reported to increase linearly with electrode area[8-9]. This apparent discrepancy can be explained by noting that the measurements were performed with electrodes of different areas. Capacitive loading noise can be expected to dominate for large electrodes because the noise PSD increases with the electrode area squared (Eq. 2), whereas the PSD due to thermal noise is only linearly proportional to electrode area (Eq. 7). Thus with large electrodes σ_I can be expected to increase linearly with electrode area. Fig. S-3 plots σ_I versus electrode area on a double-logarithmic scale for electrodes that vary in area over two orders of magnitude. Data from electrodes smaller than 2500 μm^2 are the same as depicted in Fig. 6A, and are well described by a power law with an exponent of 0.5 (dashed line) or 0.56 (solid line). On the other hand, the relationship is nearly linear for electrode areas greater than ~3000 μm^2 (dotted line).

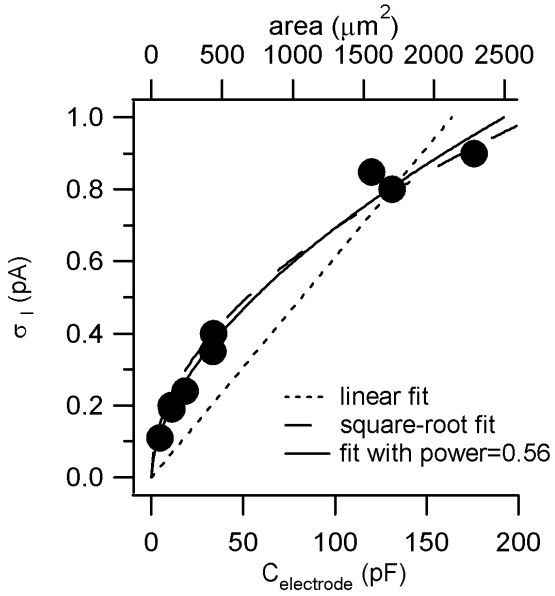

Fig. S-3. Noise standard deviation increases with the square-root of electrode area for small electrodes, but linearly with area for larger electrodes. σ_I is plotted versus electrode capacitance for ITO electrodes. The top axis converts electrode capacitance to area using the slope of 0.077 pF/μm^2 obtained from the data of Fig. S-2. The bandwidth was 1 kHz. The data for areas less than 3000 μm^2 are the same as depicted in Fig. 6A.

SUPPORTING INFORMATION DISCUSSION SECTION

Possible noise sources for amperometric measurements using microelectrodes

Whereas our results demonstrate that thermal noise at the electrode-electrolyte interface is dominant under careful fabrication and recording conditions, use of inappropriate electrode materials or insufficient insulation, or insulation with a high dielectric loss factor, will result in additional noise. Introducing a high series resistance can also produce additional thermal noise, which is why we deposit highly conductive ITO underneath the less conductive DLC electrode material.

A common additional source of current fluctuations is line (mains) interference, i.e., capacitive pickup of ac signals from lights and other equipment. This is a predictable interference, rather than random noise, and can, in principle, be eliminated through careful shielding of the experimental setup and subtraction of any residual periodic waveform from the signal. Nevertheless, even when line interference is not readily apparent by inspection of the records, we have found that it is easy for this source to be the dominant contributor to the standard deviation of the current (σ_I). Thus in the present study we use power spectral analysis to analyze noise in order to clearly separate out periodic interference and reveal the frequency dependence of the random noise that constitutes the true resolution limit for amperometric measurements.

The amplifier can also easily be a dominant noise source under certain conditions. The most appropriate amplifiers for low-current amperometric measurements of exocytosis are "patch-clamp" two-electrode potentiostats where the noise is ideally determined by the thermal noise of the feedback resistor, which is 0.5 GΩ for both the NPI VA-10 and the HEKA EPC-10 when set to the intermediate gain range. Our noise measurements were carried out using the high gain range of the EPC-10 (50 GΩ feedback resistor) in order to ensure low amplifier noise. The dashed line in Fig. 3 denotes the theoretical thermal noise of a 0.5 GΩ resistor in order to allow comparison with the intrinsic noise of the electrochemical microelectrodes. It is clear that this value of feedback resistance could be the dominant noise source for small electrodes if the bandwidth of the measurements is small (also see[10]). On the other hand, it is usually only possible to record a maximum current of ~200 pA without saturating the amplifier if a 50 GΩ feedback resistor is used. This suggests that a compromise value for the feedback resistor in the several GΩ range would be ideal for amperometric measurement of quantal exocytosis from neuroendocrine cells. Nevertheless, even a high-gain amplifier can easily be the dominant noise source as electrodes approach diameters of several μm or smaller in diameter, particularly for bandwidths < 1 kHz.

Our results demonstrate that capacitive loading of the amplifier (e_nC noise) is not the dominant noise source for microelectrodes smaller than ~2500 μm^2 under common recording conditions. In particular,

1. The experimentally measured e_nC noise with a discrete capacitor attached to the probe input is much smaller than that of an electrochemical microelectrode with a similar capacitance (Fig. 3). This is not unexpected since a theoretical calculation according to Eq. 2 suggests that e_nC noise should be small for audio-range frequencies compared to that found in electrochemical microelectrodes.
2. The current noise PSD is approximately linearly proportional to the electrode capacitance (e.g., two traces of Fig. 3). The PSD should increase with the electrode capacitance squared if e_nC noise dominates (Eq. 2). Similarly, the current noise (σ_I) scales with the square-root of area / capacitance (Fig. 6A) for smaller electrodes, whereas σ_I scales

linearly with area for larger electrodes (Fig. S-3) where e_nC noise dominates.

3. The current PSD of electrodes increases approximately linearly with frequency (Fig. 3) and the current standard deviation increases with bandwidth raised to a power slightly less than one (Fig. 6B). If e_nC noise is dominant then the PSD should increase with frequency squared (Eq. 2) and the standard deviation should increase with bandwidth raised to a power of 1.5 (combining Eq. 2 and 8).
4. Finally, the current PSD follows the Nyquist prediction for thermal noise (Eq. 3) extremely well (Fig. 4). This would not be the case if e_nC noise is dominant.

On the other hand, e_nC noise can be dominant for larger electrodes, when amplifiers with high input voltage noise are used (e.g.,[11]), or if very high bandwidths (10s of kHz) are desired.

Despite a previous suggestion[12], shot noise is unlikely to be a major source of noise for these measurements. Shot noise due to a "background" faradaic current I_{dc} produces a spectrally white (frequency-independent) current power spectral density given by:

$$S_I = 2neI_{dc}$$

where *e* is the fundamental charge of an electron and *n* is the valence of the electron transfer reaction. Thus currents greater than ~50 pA due to monovalent charge-transfer reactions are necessary to produce shot noise with a magnitude greater than the thermal noise of a cell-sized electrode or a 1 GΩ feedback resistor of a potentiostat. Appropriate polarizable electrode materials, however, have small enough background faradaic currents at the potential used for amperometric measurements (< 0.5 pA/μm^2) such that background shot noise is small compared to the thermal noise of the electrode surface.

The faradaic current that results from oxidation of transmitter on the working electrode could be an additional source of thermal noise. The faradaic current results in a diffusional or "Warburg" impedance in parallel with the double-layer electrode impedance[6]. The Warburg impedance has a magnitude that scales with $f^{-0.5}$ and a phase of -45°, i.e., it is a constant-phase-element with $\alpha = 0.5$. The physical origin of the Warburg impedance is that small fluctuations in voltage at the working electrode lead to a change in the relative concentrations of the oxidized and reduced forms of the analyte at the surface of the electrode. This, in turn, leads to changes in the faradaic current driven by diffusion from the bulk solution. Under our recording condition the voltage is held at an anodic potential far from the formal potential for the transmitter analyte in order to drive "all" transmitter reaching the electrode surface to the oxidized state to yield the amperometric current. On the other hand, the surface concentration of the reduced form is essentially zero. Under this condition, small changes in electrode potential will have little if any effect on the faradaic current, so the Warburg impedance should be very high and thus contribute little to the thermal noise of the electrode.

The dominant thermal noise likely originates from the thermal motion of ions in the frictional environment of the electrolyte-electrode interface. Rough or porous electrode materials give CPE α values of ~0.5 and prominent thermal noise because ion movements encounter friction within the pores of the electrode. Our sputter-deposited electrodes, however, are atomically smooth as verified using AFM[7]. It seems likely, however, that material- and time / frequency-dependent adsorption of ions or water to the electrode surface will present a frictional barrier to free movement of ions to result in thermal noise.

Strategies for reducing noise during amperometric recording of exocytosis

Surface-patterned electrodes provide the opportunity to carefully control electrode geometries and select from a range of materials. Our results suggest that the Constant Phase Element parameter α is critical in determining noise performance. A smoother electrode surface results in better (closer to unity) α values, and materials such as ITO have better noise performance than Au, although the amperometric signal in response to catecholamine release is also smaller on ITO[13], therefore further study is needed to quantify the signal-to-noise ratio of various electrode materials. DLC:N appears to have a good signal-to-noise ratio and is reasonably transparent to allow imaging of cells over the electrodes[1, 9, 14] and it also promotes cell adhesion to electrodes[15-16].

Current noise (σ_I) increases with the square root of the area of the working electrode therefore reducing the electrode size reduces noise[10]. However, further gains in noise performance are difficult to achieve for electrodes smaller than several μm in diameter because the potentiostat or other noise sources will become dominant and smaller electrodes will detect fewer exocytosis events and will not capture all the transmitter released from an individual vesicle[17]. Therefore an electrode diameter of several μm is appropriate for optimum noise when recording quantal exocytosis from neuroendocrine cells, whereas cell-sized electrodes are convenient to trade off higher noise for more captured events (e.g., [18]).

Properly shielding connections to the microelectrodes is important to reduce pickup of line interference and proper insulation of inactive areas of the conductive material is essential, although a variety of insulating materials (e.g., SU8 thick photoresist[18], Teflon AF[16], parylene C[19], poly(acrylic−carboxylic acid)[20] give good results .

Ideally, a potentiostat should be selected with a feedback resistor in the low GΩ range for amperometric measurements of exocytosis from neuroendocrine cells. Finally, since the electrode noise is "blue" (increases with frequency) rather than spectrally white, it is important to limit the bandwidth of the recording to the minimum necessary to resolve spike features of interest.

SUPPORTING INFORMATION REFERENCES

1. X. Chen, Y. Gao, M. Hossain, S. Gangopadhyay and K. D. Gillis, *Lab on a Chip - Miniaturisation for Chemistry and Biology*, 2007, **8**, 161-169.
2. S. Barizuddin, X. Liu, J. C. Mathai, M. Hossain, K. D. Gillis and S. Gangopadhyay, *ACS Chem Neurosci*, 2010, **1**, 590-597.
3. K. D. Gillis, *Pflugers Archiv European Journal of Physiology*, 2000, **439**, 655-664.
4. M. Lindau and E. Neher, *Pflugers Archiv European Journal of Physiology*, 1988, **411**, 137-146.
5. M. Pusch and E. Neher, *Pflugers Archiv European Journal of Physiology*, 1988, **411**, 204-211.
6. A. J. Bard and L. R. Faulkner, *Electrochemical Methods: Fundamentals and Applications*, Second edn., Wiley & Sons, New York, 2001.
7. Y. Gao, X. Chen, S. Gupta, K. D. Gillis and S. Gangopadhyay, *Biomedical Microdevices*, 2008, **10**, 623-629.
8. J. T. Long and S. G. Weber, *Anal Chem*, 1988, **60**, 2309-2311.
9. X. Sun and K. D. Gillis, *Analytical Chemistry*, 2006, **78**, 2521-2525.
10. A. Schulte and R. H. Chow, *Analytical Chemistry*, 1998, **70**, 985-990.
11. J. T. Long and S. G. Weber, *Analytical Chemistry*, 1988, **60**, 2309-2311.

12. E. Neher and R. H. Chow, *Bioelectrochemistry and Bioenergetics*, 1995, **38**, 251-253.
13. K. Kisler, B. Kim, K. Berberian, Q. Fang and M. Lindau, *Biophys J*, 2007, **92**, 83a.
14. C. Amatore, S. Arbault, Y. Chen, C. Crozatier, F. Lema ître and Y. Verchier, *Angewandte Chemie - International Edition*, 2006, **45**, 4000-4003.
15. A. Sen, S. Barizuddin, M. Hossain, L. Polo-Parada, K. D. Gillis and S. Gangopadhyay, *Biomaterials*, 2009, **30**, 1604-1612.
16. S. Barizuddin, X. Liu, J. C. Mathai, M. Hossain, K. D. Gillis and S. Gangopadhyay, *ACS Chemical Neuroscience*, 2010, **1**, 590-597.
17. C. Amatore, S. Arbault, Y. Bouret, M. Guille, F. Lemaitre and Y. Verchier, *Anal Chem*, 2009, **81**, 3087-3093.
18. X. Liu, S. Barizuddin, W. Shin, C. J. Mathai, S. Gangopadhyay and K. D. Gillis, *Analytical Chemistry*, 2011, **83**, 2445-2451.
19. K. C. Morton, C. A. Morris, M. A. Derylo, R. Thakar and L. A. Baker, *Analytical Chemistry*, 2011, **83**, 5447-5452.
20. A. Schulte and R. H. Chow, *Anal Chem*, 1996, **68**, 3054 - 3058.